Characterization of Crystalline Drug Nanoparticles Using Atomic Force Microscopy and Complementary Techniques

Huaiqiu Galen Shi,[1,5] Leon Farber,[2] James N. Michaels,[2] Allison Dickey,[3] Karen C. Thompson,[1] Suhas D. Shelukar,[1] Patricia N. Hurter,[1] Scott D. Reynolds,[1] and Michael J. Kaufman[1,4]

Received November 12, 2002; accepted November 19, 2002

Purpose. The purpose of this work was to image crystalline drug nanoparticles from a liquid dispersion and in a solid dosage form for the determination of size, shape, and distribution.

Methods. Crystalline drug nanoparticles were adsorbed from a colloidal dispersion on glass for atomic force microscopy (AFM) imaging. Nanoparticles that were spray coated onto a host bead were exposed by ultramicrotomy for scanning electron microscopy and AFM examination.

Results. The adsorbed drug nanoparticles were measured by AFM to have a mean diameter of 95 nm and an average aspect ratio of 1.3. Nanoparticles observed in the solid dosage form had a size and shape similar to drug nanoparticles in the dispersion. Particle size distribution from AFM measurement agreed well with data from field emission scanning electron microscopy, static light scattering, and X-ray powder diffraction.

Conclusions. AFM is demonstrated to be a valuable tool in visualization and quantification of drug nanoparticle crystals in formulations. In addition to accurate size measurement, AFM readily provides shape and structural information of nanoparticles, which cannot be obtained by light scattering. Ultramicrotomy is a good sample preparation method to expose the interior of solid dosage forms with minimal structural alteration for microscopic examination.

KEY WORDS: atomic force microscopy; nanoparticle; ultramicrotomy; scanning electron microscopy, light scattering.

INTRODUCTION

It has been a challenge in pharmaceutical sciences to improve the bioavailability of poorly water soluble drugs. A promising approach from the formulation perspective is to reduce drug particle size to the submicron or nanometer regime (1). The consequent increase in particle surface area leads to an increase in dissolution rate, which may enhance the drug bioavailability, if it is limited by dissolution rate.

Nanocrystal™ is an enabling technology licensed to Merck from Elan/Nanosystems (King of Prussia, PA, USA) to mill drug particles to 200 nm or less (2,3). Nanoparticle formulations are being developed for several Merck compounds that are poorly soluble. It is critical to visualize colloidal drug in a milled dispersion because this can verify particle size distribution determined typically by light scattering and obtain shape and structural information that is unavailable with other techniques. What is equally important is to characterize drug nanoparticles in solid dosage forms for their size, shape, and spatial distribution, which is related to upstream processing and dosage performance. Among microscopy techniques, transmission electron microscopy and scanning electron microscopy (SEM) have been used for imaging drug nanoparticles (1,2).

Since its introduction in 1982 (4), scanning probe microscopy (SPM) has rapidly evolved into a family of powerful techniques for high resolution imaging and high sensitivity spectroscopy. Atomic force microscopy (AFM) is the most versatile branch of SPM developed for nonconductive samples (5). It is well known for its nanometer resolution and *in situ* imaging capability in liquid, air, or vacuum. AFM has found various applications in pharmaceutical research, including drug polymorphic discrimination (6,7), determination of intrinsic dissolution rate of crystal planes (8), quantitation of adhesion between powders (9,10) and particles and gelatin surfaces (11), and surface roughness measurement of particles (12). AFM was used to image solid lipid nanoparticles, a controlled release drug carrier system composed of lipid, poloxamer, and amorphous drug (13). Nonetheless, there has been no report, to the authors' knowledge, on AFM characterization of nanoparticle drug crystals in dosage forms or in intermediate formulations.

The goal of this investigation was to use an AFM to examine drug nanocrystals contained in a colloidal coating dispersion and on cellulose beads coated with the dispersion. The particle size determined from AFM images is compared with the results of light scattering, SEM, and X-ray powder diffraction (XRPD) measurements. Ultramicrotomy was applied to cleave open the beads embedded in epoxy. This procedure minimizes structural damage to the beads and renders a smooth cross section of the coating that is ideal for imaging.

MATERIALS AND METHODS

Nanoparticles Adsorbed from Dispersion

The colloidal dispersion contained drug nanoparticles in an aqueous solution containing a polymer and a small amount of surfactant. One hundred microliters of the dispersion was placed on a clean glass cover slide, which was thoroughly rinsed with deionized water and dried under a nitrogen stream.

Light Scattering of Colloidal Dispersion

Particle sizing of the dispersion was conducted using a Coulter LS-230. The angular light intensity was measured at 750 nm and polarization intensity differential scattering was measured at 450, 600, and 900 nm. The particle size distribution was calculated on a volume weighted basis by processing the data collected with an optical model, which was built using the real and imaginary refractive index components for the drug and took into account Mie theory and polarization intensity differences for light scattering.

[1] Pharmaceutical R&D, MRL, Merck & Co., Inc., West Point, Pennsylvania 19486

[2] Pharmaceutical Materials Laboratory, Merck & Co., Inc., West Point, Pennsylvania 19486

[3] Department of Chemical Engineering, Pennsylvania State University, University Park, Pennsylvania 16802

[4] Current address: Millennium Pharmaceuticals, Inc., Cambridge, Massacheusetts 02139

[5] To whom correspondence should be addressed. (e-mail: galen_shi@merck.com)

0724-8741/03/0300-0479/0 © 2003 Plenum Publishing Corporation

Spray Coated Beads for Ultramicrotomy

The drug nanoparticle dispersion was spray coated onto host beads of microcrystalline cellulose. The beads were embedded in a two component epoxy (resin 811-563-105 and hardener 811-563-106 from Leco, St. Joseph, MI, USA), which was cured at 60°C for 20 h. The embedded beads were cut at room temperature to expose the interior with an Reichert-Jung Ultracut E ultramicrotome (Leica, Austria) using a Histo 45° diamond knife (Diatome, Switzerland).

AFM Operation and Image Analysis

The glass coverslide with adsorbed drug nanoparticles and the ultramicrotomed beads were examined with a Dimension 3100 SPM (Digital Instruments, Santa Barbara, CA, USA). The instrument was operated in air in tapping mode with a TESP-etched silicon probe (Digital Instruments). Both height and phase images were collected and analyzed with Nanoscope III software (Digital Instruments). Calibration studies were conducted with monodisperse colloidal particles and a calibration grid to ensure accuracy. AFM images were imported into Image-Pro image analysis software (Media Cybernetics, Silver Spring, MA, USA) to extract particle size distribution and shape information. The mean diameter of a particle was determined by averaging diameters measured at 2° intervals joining two outline points and passing through the centroid using the software algorithm. The aspect ratio value reports the ratio between the major axis and the minor axis of the ellipse equivalent to the particle (i.e., an ellipse with the same area, first and second degree moments).

Environmental SEM and Field Emission (FE) SEM Imaging

The cross sections of ultramicrotomed beads were examined using an environmental SEM Philips Electroscan 2020. The electron accelerating voltage was 20 kV, and the water vapor pressure was 4 torr. A cross section of the bead was also sputter coated with gold using a vacuum coater (SPI, West Chester, PA, USA), and then imaged using a JEOL 6300 SEM equipped with a field emission gun operated at 5 KeV.

XRPD

The drug-coated beads were immersed in water (1:2 ratio of beads to water by volume) and sonicated for 10 min. This resulted in dissolution of the coating and formation of a drug suspension for XRPD analysis. The procedure eliminated peaks from other crystalline components in the coating that interfere with drug diffraction peaks and would make the subsequent quantitative analysis more difficult. Drug crystal powder was used as a reference. The effect of preferred orientation in the powder sample was minimized by hand grinding the powder for 20 s. X-ray diffraction spectra were measured with a Siemens D5000 diffractometer equipped with a parallel beam optical system using Cu Kα irradiation. A scanning rate of 0.2°/min and 0.02° step was used to collect spectra. Peaks were analyzed using the standard Siemens software package.

RESULTS

Nanoparticles from Colloidal Dispersion

Colloidal particles, such as proteins, often adsorb from a solution to surfaces via hydrophobic interactions or electrostatic forces (14). It has been standard practice to use AFM to image macromolecules or nanoparticles adsorbed to a smooth substrate like glass or mica (15). Drug nanoparticles were found to adsorb readily to glass from a liquid dispersion, possibly with surface adsorbed polymer and surfactant. Figure 1 shows that hundreds of individual drug nanoparticles, appearing as bright spots, adsorbed onto glass, which is the dark background. The surface coverage of nanoparticles was relatively uniform and could be controlled by varying the dilution of the dispersion. The nanoparticles apparently had a fairly narrow size distribution. Figure 2a is a magnified, three-dimensional picture of surface-adsorbed nanoparticles. It shows that the majority of colloidal particles on glass were separated from each other, which suggests that these nanoparticles were probably stabilized against agglomeration in the milled dispersion.

The lateral dimensions of the nanoparticles (n = 239) observed in Fig. 2a were analyzed quantitatively. The number-averaged particle size distribution was plotted geometrically on a logarithmic scale and compared with the number based distribution determined by light scattering for the same batch of dispersion, as shown in Fig. 2b. The AFM measurement provided a distribution of particle size similar to that from the light scattering experiment. The median diameter from AFM measurement is 87 nm and the mean diameter is 95 nm. This result agrees reasonably well with 73 nm and 80 nm as the median and the mean diameters respectively from light scattering, although the two techniques measure conceptually different representations of particle size. The AFM generated particle size distribution curve is not as smooth as that from light scattering, because the former has a sampling size several orders of magnitude smaller than the latter. It is noted that AFM was able to detect particles less than 40 nm

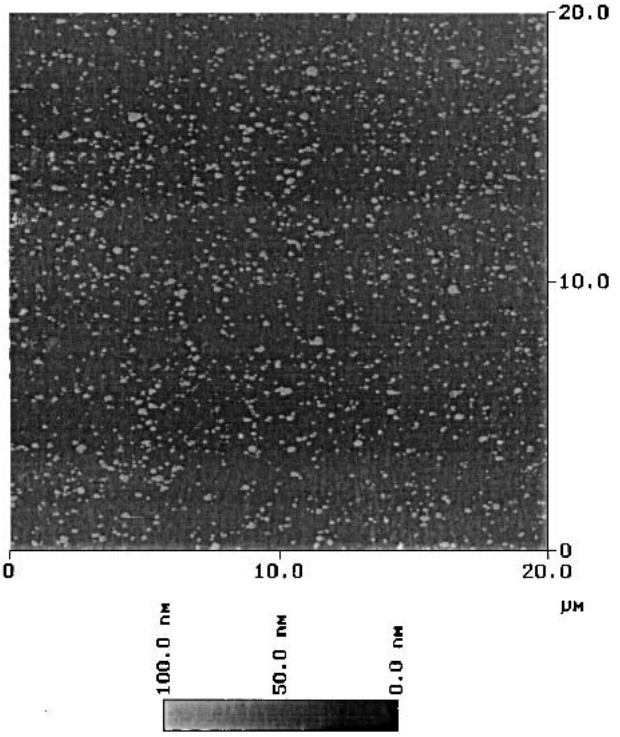

Fig. 1. Drug nanoparticles adsorbed on glass from a diluted dispersion as imaged by tapping-mode atomic force microscopy in air.

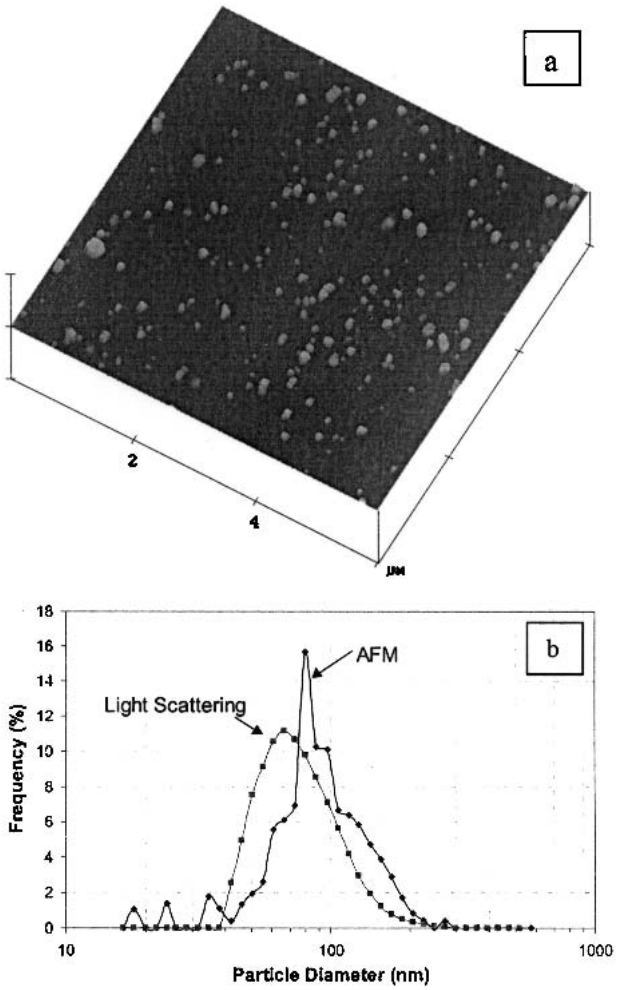

Fig. 2. Three-dimensional atomic force microscopy image of colloidal drug particles adsorbed on glass (a) with a scan size of 6 μm and (b) the number-weighted particle size distributions of nanoparticles in a milled dispersion as determined by static light scattering and atomic force microscopy.

whereas static light scattering could not. Line profile analysis shows that the height of most nanoparticles is in the range of 30–200 nm. The heights of adsorbed nanoparticles are comparable overall to their lateral dimensions, suggesting that the nanoparticles probably have a spherical or cubic morphology rather than a flaky morphology.

An advantage of microscopy is that pictures are rich in shape and structural information. The average aspect ratio of nanoparticles in Fig. 2a was determined to be 1.3 ± 0.2. The higher magnification image in Fig. 3 demonstrates that drug nanoparticles are quasispherical or cubic. It also shows that although many colloidal drug particles are primary particles that are well separated, some nanoparticles are in close proximity to each other or even in contact.

Nanoparticles in Spray-Coated Beads

An ultramicrotome was used to cut open the nanoparticle-coated beads that were embedded in epoxy to expose the interior. The environmental SEM picture of the cross-sectioned bead in Fig. 4 clearly shows the structures of the drug coating and the core of the cellulose bead. The coating

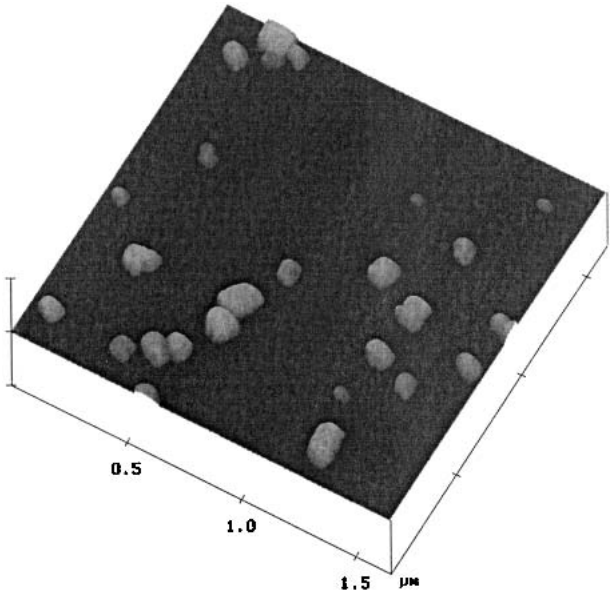

Fig. 3. Three-dimensional atomic force microscopy image of nanoparticles adsorbed on glass with a scan size of 1.7 μm.

has many macropores ranging from 1 to 30 μm in size. These pores were possibly formed during drying of the spray-coated layers. The distribution of pores is relatively uniform across the radius of the bead. In comparison, the cellulose core is denser, with only a few small pores typically less than 5 μm in diameter. The microtomed cross section is smooth except for occasional cutting marks resulting from imperfections of the cutting knife. The random orientations of the coating pores demonstrate that microtoming did not cause significant structural damage to the coated bead.

A crack was observed in Fig. 4 extending from the outer surface of the coating to the surface of the core bead. The crack is about 10 μm wide at the coating surface and around 2 μm wide near the core, which suggests that the crack possibly propagated from the surface toward the core. It is evident that cutting did not induce the crack because it was filled with epoxy that was cured before microtoming. It was prob-

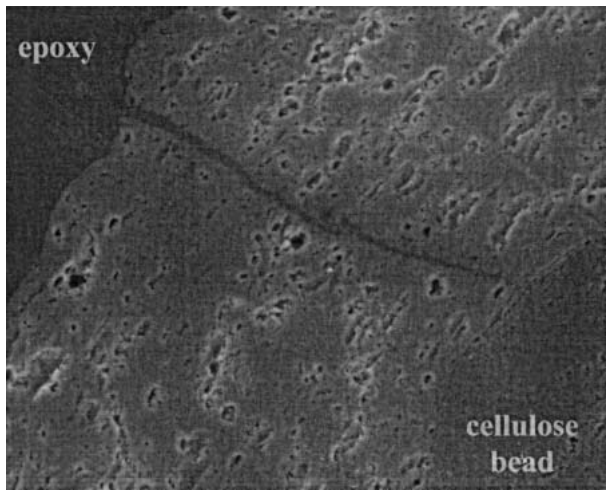

Fig. 4. Environmental scanning electron microscopy image of the cross section of an ultramicrotomed, drug-coated bead that was embedded in epoxy.

ably not caused by embedding in epoxy either, because similar cracks were found on the surface of other drug-coated beads.

AFM characterization of drug-coated beads was conducted on the flat areas of the cross sections and inside the pores. Figure 5 shows that particles of comparable size to the drug nanoparticles are scattered in a matrix as found in both regions. The particles measured in Fig. 5 have a mean diameter of 83 nm, which is smaller than the particle size of 95 nm determined by AFM for drug nanoparticles from the milled dispersion. This difference could be because the particles are partially embedded in the matrix, exposing only a portion of the surface for imaging, and thus the true size is underestimated. The average aspect ratio of nanoparticles in the coated beads is 1.4 ± 0.3, in good agreement with 1.3 ± 0.2 for the nanoparticles in the milled dispersion. Because the size and aspect ratio of these particles are consistent with those of drug nanoparticles, we believe the particles observed in coated beads are drug nanoparticles.

The AFM measurement of the size of drug nanoparticles in coated beads is also supported by FE SEM pictures of cross-sectioned beads in addition to light-scattering and XRPD results of redispersed nanoparticles. As shown in Fig. 6, drug nanoparticles can be easily recognized in FE SEM micrographs because of the characteristic contrast. The size of the particles is in the range of 15–300 nm, with typical particle size of about 100 nm. Light-scattering measurements performed for the redispersion of coated beads also indicate that the nanoparticles remained approximately the same size as those in the milled dispersion.

Figure 7 shows the X-ray diffraction patterns for the drug nanoparticle suspension redispersed from the coated beads and the reference microns-sized drug crystals. The peak at

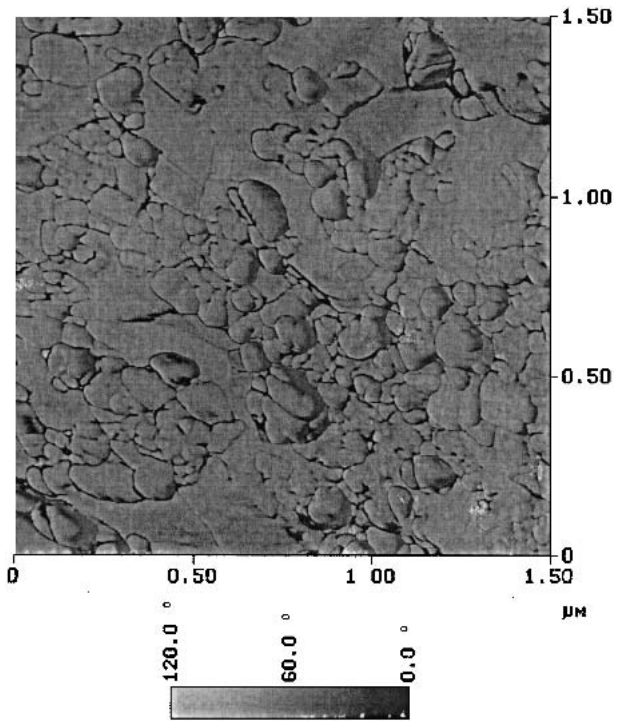

Fig. 5. Tapping-mode atomic force microscopy phase image of the cross section of a drug-coated bead.

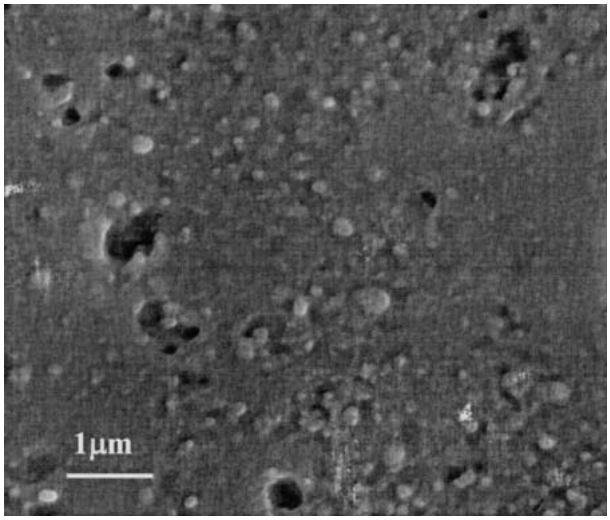

Fig. 6. Field emission scanning electron microscopy image of the cross section of a drug-coated bead.

20.7° of 2θ is broadened for the nanoparticle suspension. Particle size is calculated from peak broadening according to the equation below:

$$D = \lambda/(\beta\cos\theta),$$

where D is the mean particle size, λ is the radiation wavelength, θ is the diffraction angle, and β is peak broadening expressed in radians, as calculated from the following equation:

$$\beta = (\beta_1^2 - \beta_0^2)^{1/2}$$

where β_1 and β_0 are full width at half maxima (FWHM) of the peak in samples with small and large particles, respectively (16). The FWHM values for drug nanoparticle suspension and the reference powder are 0.208 and 0.180, respectively. Because the particle size of the reference powder is larger than 500 nm and the peak is not considered broadened, the size of drug nanoparticle in suspension is thus calculated as 84 nm.

AFM images show that the microscale morphology and drug nanoparticle distribution is not homogeneous throughout the coating. The particle coverage in some areas is smaller than in other areas, as shown in Fig. 8, which is confirmed by FE SEM pictures. However, there is no obvious trend ob-

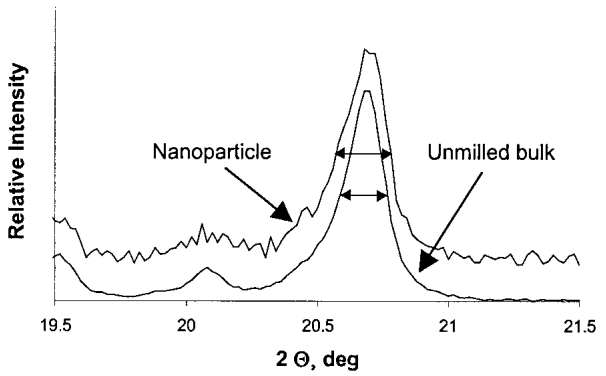

Fig. 7. Typical X-ray powder diffraction patterns of drug nanoparticles redispersed from the coated beads and reference bulk drug.

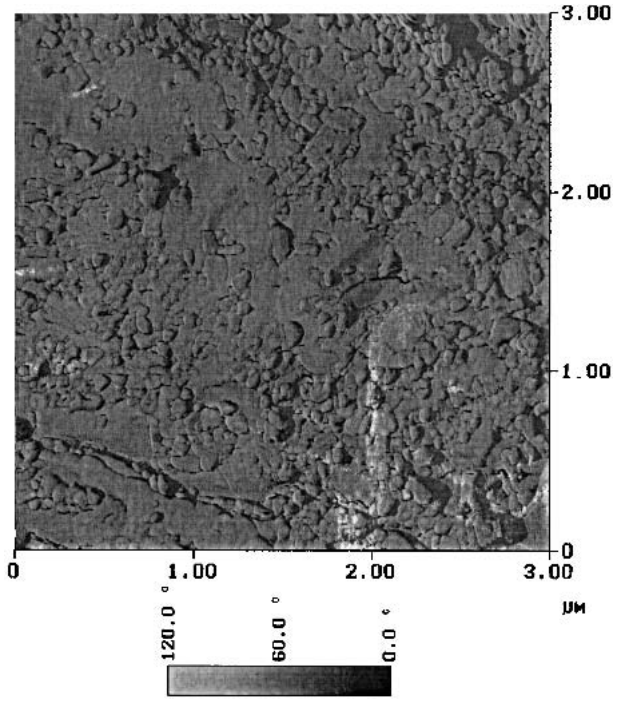

Fig. 8. Tapping-mode atomic force microscopy phase image of a region in the cross section that has an inhomogeneous distribution of nanoparticles.

served in the nanoparticle distribution across the radius of the coated bead.

DISCUSSION

Height images of tapping-mode AFM were captured for generating three-dimensional pictures of nanoparticles adsorbed on glass from the milled dispersion. One concern with nanoparticle adsorption is that a particular population of the dispersion may preferentially adsorb onto the glass to present an unrepresentative sample. We believe this preferential adsorption did not occur in our experiments because in imaging other drug nanoparticles made by a different milling process, a much broader size distribution of nanoparticles was observed including large agglomerates and tiny (less than 10 nm) particles. Thus, both large and small particles can adsorb to glass if they are present in the dispersion.

Phase images in tapping mode were used for quantification of nanoparticles in coated beads because it is difficult to reveal small topographic changes in the height image of cross sections. In tapping mode the AFM tip is oscillated to be in contact with the sample surface intermittently, minimizing sample damage associated with dragging the AFM probe over the sample in contact mode imaging. Phase images capture the phase lag signal of the cantilever/tip oscillation, and the contrast is reflective of a multitude of energy dissipation effects at the tip-sample interaction point, such as topography and material properties. In this application, our phase images reflect mostly, and accentuate, surface topographical change. They serve as an edge enhancement tool for outlining the silhouettes of drug nanoparticles.

Ultramicrotomy was used to cleave drug-coated beads in a controlled and unbiased manner to expose the interior for AFM and SEM imaging. A microtome is traditionally the tool for sectioning biologic samples or polymers for transmission electron microscopy and optical microscopy (17). An ultramicrotome can achieve slices thinner than 100 nm. In this case, the smooth sample surface remaining after cutting is used for microscopy instead of a thin slice. The coating is a hard composite material, thus the cross-sectioned surface is probably exposed by a combination of cutting and controlled fracture. AFM and FE SEM imaging of the cross section shows that microtoming did not alter the sample structure noticeably because drug nanoparticles were not found to be dragged along the cutting direction. The nanoparticles usually protrude out of the cutting plane, suggesting that they were not cleaved into halves but were exposed by knife cutting/fracturing the surrounding matrix. Smooth and flat surfaces are suitable not only for microscopy but for chemical imaging analysis, such as time-of-flight secondary ion mass spectrometry, micro-Raman, and infrared and near-infrared microprobes, where signals received can be influenced by sample topography.

Good agreement was observed between particle size distributions determined by image analysis of AFM images of nanoparticles adsorbed on glass and by static light scattering of the nanoparticle dispersion. This quantitative agreement was realized because the nanoparticles were relatively monodisperse and roughly spherical in shape. The nanoparticle size measured by AFM appears to be larger than light-scattering results, partially because the AFM tip broadens surface peaks that are of similar size as the probe (18–20). This tip dilation effect was found to be significant when our control samples for AFM imaging, monodisperse colloidal particles, were less than 50 nm in diameter. In general, AFM and light scattering are complementary techniques for quantification of nanoparticle size. Static light scattering measures the equivalent spherical diameter based on volume of particles dispersed in a (usually) liquid medium, whereas image analysis of AFMs directly measures the geometric diameter of particles in air (for simplicity in this experiment) or in a liquid, such as the milled dispersion. Static light scattering cannot measure accurately particles smaller than 50 nm or particles of irregular shape, such as needles, and it tends to be biased against small particles in a polydisperse mixture, whereas AFM can measure much smaller features of various shapes; however, the resulting image is a convolution of sample topography and tip geometry. AFM can also provide structural and shape information of the particles analyzed, which is not available from conventional light-scattering measurements. Nonetheless, light scattering typically samples a much greater number of particles than AFM, and data acquisition and analysis for the former is normally faster than the latter.

AFM, environmental SEM, and FE SEM were the microscopic techniques used in this study. Comparable high resolution was achieved with AFM and FE SEM, whereas individual nanoparticles were not resolved by environmental SEM. FE SEM has the advantages of being able to achieve a large field of view, large depth of field, and fast image acquisition, but it requires conductive metal coating of the sample and a high vacuum operating environment. In comparison, AFM can examine uncoated insulating samples in air or in liquid. Given the complementary nature of these two techniques (21,22), it is advantageous to apply both for characterization of drug nanoparticles in their formulations.

ACKNOWLEDGMENTS

The authors acknowledge the Penn Regional Materials Characterization Facility of the University of Pennsylvania for providing the opportunity to use FE-SEM and Helmut Potzig at Microscopical Optical Consulting Inc. and Patricia J. Masarachia at Merck for the access to Leica/Reichert-Jung ultramicrotomes.

REFERENCES

1. R. H. Muller, C. Jacobs, and O. Kayser. Nanosuspensions as particulate drug formulations in therapy rationale for development and what we can expect for the future. *Adv. Drug Deliv. Rev.* **47**:3–19 (2001).
2. G. C. Liversidge and P. Conzentino. Drug particle size reduction for decreasing gastric irritancy and enhancing absorption of naproxen in rats. *Int. J. Pharm.* **125**:309–313 (1995).
3. G. C. Liversidge and K. C. Cundy. Particle size reduction for improvement of oral bioavailability of hydrophobic drugs. I. Absolute oral bioavailability of nanocrystalline danazole in beagle dogs. *Int. J. Pharm.* **127**:309–313 (1995).
4. G. Binnig and H. Rohrer. Scanning tunneling microscopy. *Helv. Phys. Acta* **55**:726–735 (1982).
5. G. Binnig and C. Quate. Atomic force microscope. *Phys. Rev. Lett.* **56**:930–933 (1986).
6. A. Danesh, X. Chen, M. C. Davies, C. J. Roberts, G. H. W. Sanders, S. J. B. Tendlers, and P. M. Williams. Polymorphic discrimination using atomic force microscopy: distinguishing between two polymorphs of the drug cimetidine. *Langmuir* **16**:866–870 (2000).
7. A. Danesh, X. Chen, M. C. Davies, C. J. Roberts, G. H. W. Sanders, S. J. B. Tendlers, P M. Williams, and M. J. Wilkins. The discrimination of drug polymorphic forms from single crystals using atomic force microscopy. *Pharm. Res.* **17**:887–890 (2000).
8. A. Danesh, S. D. Cornnell, M. C. Davies, C. J. Roberts, S. J. B. Tendlers, P. M. Williams, and M. J. Wilkins. An *in situ* dissolution study of aspirin crystal planes (100) and (001) by atomic force microscopy. *Pharm. Res.* **18**:299–303 (2001).
9. M. D. Louey, P. Mulvaney, and P. J. Stewart. Characterization of adhesional properties of lactose carriers using atomic force microscopy. *J. Pharm. Biomed. Anal.* **25**:559–567 (2001).
10. U. Sindel and J. Zimmermann. Measurement of interaction forces between individual powder particles using an atomic force microscope. *Powder Technol.* **117**:247–254 (2001).
11. T. H. Ibrahim, T. R. Burk, F. M. Etzler, and R. D. Neuman. Direct adhesion measurements of pharmaceutical particles to gelatin capsule surfaces. *J. Adhesion Sci. Technol.* **14**:1225–1242 (2000).
12. T. Li and K. Park. Fractal analysis of pharmaceutical particles by atomic force microscopy. *Pharm. Res.* **15**:1222–1232 (1998).
13. A. zur Muhlen, E. zur Muhlen, H. Niehus, and W. Mehnert. Atomic force microscopy studies of solid lipid nanoparticles. *Pharm. Res.* **13**:1411–1416 (1996).
14. J. D. Andrade. Principles of protein adsorption. In J. D. Andrade (ed.), *Surface and Interfacial Aspects of Biomedical Polymers: Protein Adsorption II*, Plenum Press, New York, 1985, pp. 1–80.
15. Z. Shao, J. Mou, D. M. Czajkowsky, and J. Yang. and J. Yuan. Biological atomic force microscopy: what is achieved and what is needed. *Adv. Phys.* **45**:1–86 (1996).
16. B. D. Cullity. *Elements of X-Ray Diffraction*, Addison-Wesley, Reading, Massachusetts, 1978.
17. L. C. Sawyer and D. T. Grubb. *Polymer Microscopy.* Chapman and Hall, New York, 1987.
18. J. S. Villarrubia. Morphological estimation of tip geometry for scanning probe microscopy. *Surface Sci.* **321**:287–300 (1994).
19. N. Bonnet, S. Dongmo, P. Vautrot, and M. Troyon. A mathematical morphology approach to image formation and image restoration in scanning tunneling and atomic force microscopies. *Microscopy Microanalysis Microstructures* **5**:477–487 (1994).
20. D. L. Wilson, K. S. Kump, S. J. Eppell, and R. E. Marchant. Morphological restoration of atomic force microscopy images. *Langmuir* **11**:265–272 (1995).
21. P. Russel and D. Batchelor. SEM and AFM: complementary techniques for surface investigations. *Microscopy Analysis* **49**:5–8 (2001).
22. R. Nessler. Scanning probe technologies: scanning electron microscopy and scanning probe microscopy. *Scanning* **21**:137 (1999).